ORF3c is expressed in SARS-CoV-2 infected cells and suppresses immune activation by inhibiting innate sensing

Martin Müller[1], Alexandra Herrmann[2], Shigeru Fujita[3,4], Keiya Uriu[3,4], Carolin Kruth[1], Adam Strange[3], Jan E. Kolberg[1], Markus Schneider[1], Jumpei Ito[3], Armin Ensser[2], The Genotype to Phenotype Japan (G2P-Japan) Consortium, Kei Sato[3,4,5,6,7,8], Daniel Sauter[1,3,9,*]

[1]Institute for Medical Virology and Epidemiology of Viral Diseases, University Hospital Tübingen, 72076 Tübingen, Germany

[2]Institute for Clinical and Molecular Virology, University Hospital, Friedrich-Alexander-Universität Erlangen-Nürnberg, 91054 Erlangen, Germany

[3]Division of Systems Virology, Department of Microbiology and Immunology, The Institute of Medical Science, The University of Tokyo, Minato-ku, Tokyo, Japan

[4]Graduate School of Medicine, The University of Tokyo, Minato-ku, Tokyo, Japan

[5]International Research Center for Infectious Diseases, The Institute of Medical Science, The University of Tokyo, Minato-ku, Tokyo, Japan

[6]International Vaccine Design Center, The Institute of Medical Science, The University of Tokyo, Minato-ku, Tokyo, Japan

[7]Graduate School of Frontier Sciences, The University of Tokyo, Kashiwa, Chiba, Japan

[8]CREST, Japan Science and Technology Agency, Kawaguchi, Saitama, Japan

[9]Lead contact

***Correspondence**: daniel.sauter@med.uni-tuebingen.de

ABSTRACT

SARS-CoV-2 proteins are translated from subgenomic RNAs (sgRNAs). While most of these sgRNAs are monocistronic, some viral mRNAs encode more than one protein. For example, the *ORF3a* sgRNA also encodes ORF3c, an enigmatic 41-amino acid peptide. Here, we show that ORF3c is expressed in SARS-CoV-2 infected cells and suppresses RIG-I- and MDA5-mediated immune activation and IFN-β induction. Mechanistic analyses revealed that ORF3c interacts with the signaling adaptor MAVS, induces its C-terminal cleavage and inhibits the interaction of RIG-I with MAVS. The immunosuppressive activity of ORF3c is conserved among members of the subgenus sarbecovirus, including SARS-CoV and coronaviruses isolated from bats. Notably, however, the SARS-CoV-2 delta and kappa variants harbor premature stop codons in ORF3c demonstrating that this reading frame is not essential for efficient viral replication *in vivo* and likely compensated by other viral proteins. In agreement with this, disruption of ORF3c did not significantly affect SARS-CoV-2 replication in CaCo-2 or CaLu-3 cells. In summary, we here identify ORF3c as an immune evasion factor of SARS-CoV-2 that suppresses innate sensing in infected cells.

39 **INTRODUCTION**

40 Since the emergence of the COVID-19 pandemic, all canonical proteins of SARS-CoV-2 have
41 been extensively characterized for their expression, structure and function. In addition to its
42 prototypical genes, however, SARS-CoV-2 harbors several smaller open reading frames
43 (ORFs) that frequently overlap with other ORFs and may also contribute to efficient viral
44 replication. For example, the ORF3b peptide encoded by *ORF3a* subgenomic RNA (sgRNA)
45 was shown to suppress the induction of type I interferon (IFN) [1]. Intriguingly, naturally
46 occurring variants of ORF3b differ in their immunosuppressive activity and may be responsible
47 for phenotypic differences between SARS-CoV and SARS-CoV-2 [1]. Moreover, several short
48 upstream ORFs (uORFs) have been suggested to regulate translation of downstream genes such
49 as *ORF7b* [2]. Thus, non-canonical ORFs of SARS-CoV-2 may also be important determinants
50 of viral immune evasion, spread and/or pathogenicity.

51 Nevertheless, most of the cryptic ORFs of SARS-CoV-2 remain poorly characterized, and
52 several open questions remain: Do they encode proteins or are they merely a result of selection
53 pressures acting on overlapping reading frames? Do these ORFs exert any regulatory activity,
54 e.g. by modulating translation of downstream ORFs via leaky scanning or ribosomal re-
55 initiation? Do they code for functional proteins that contribute to efficient immune evasion
56 and/or replication of SARS-CoV-2? Are the respective peptides or proteins immunogenic?

57 One interesting cryptic open reading frame is *ORF3c*, located at nt 25457-25579 of the Wuhan-
58 Hu-1 reference genome. This ORF was independently described by different groups and has
59 received several alternative names: ORF3c [3, 4], ORF3h (for hypothetical) [5], 3a.iORF1 [2],
60 and ORF3b [6]. Following the homology-based nomenclature proposed by Jungreis and
61 colleagues [7], we will refer to this open reading frame as *ORF3c* hereafter. Like *ORF3b*,
62 *ORF3c* is one of several open reading frames overlapping with *ORF3a*. *In silico* analyses
63 suggested that the respective ORF3c protein may harbor a transmembrane domain [3] and act

64 as a viroporin [5]. Nevertheless, its expression in infected cells, as well as its exact function and
65 relevance for viral replication have remained unclear.
66 Here, we show that SARS-CoV-2 ORF3c encodes a stable 41-amino acid peptide that is
67 expressed in virally infected cells and suppresses the induction of IFN-β expression.
68 Mechanistic analyses revealed that it inhibits innate sensing induced by RIG-I and MDA5, and
69 interacts with the downstream adaptor protein MAVS. Furthermore, it inhibits the interaction
70 of RIG-I with MAVS and induces proteolytic cleavage of MAVS. In line with a relevant
71 function *in vivo*, ORF3c orthologs from different sarbecoviruses share this immunosuppressive
72 activity. However, we also identify SARS-CoV-2 lineages that spread efficiently in the human
73 population despite premature stop codons in their *ORF3c* genes. Furthermore, disruption of
74 *ORF3c* did not affect SARS-CoV-2 replication in CaCo-2 and CaLu-3 cells. Thus, our findings
75 identify ORF3c as an immune evasion factor that inhibits innate sensing cascades, but is not
76 essential for efficient viral replication.
77

78 # RESULTS

79 **SARS-CoV-2 *ORF3c* encodes a peptide suppressing IFN-β promoter activation**

80 The *ORF3a* gene of the SARS-CoV-2 reference genome Wuhan-Hu-1 overlaps with several
81 shorter open reading frames that have the potential to encode for peptides of at least 10 amino
82 acids in length (Fig 1A). Translation initiation downstream of the start codon of *ORF3a* may
83 be enabled via non-canonical translation mechanisms, such as leaky scanning, ribosomal
84 shunting and/or re-initiation [8]. In line with this, the start codon of ORF3c is part of a strong
85 Kozak sequence, and *in silico* analyses predict ORF3c expression from the ORF3a sgRNA via
86 leaky scanning [9] (Fig 1B). Indeed, ribosome profiling and HLA-II immunopeptidome studies
87 suggested that *ORF3c* is translated in SARS-CoV-2-infected cells [2, 10]. The same study also
88 found evidence for translation of *ORF3d-2* [2], which is in agreement with the detection of
89 ORF3d-specific antibodies in sera from previously SARS-CoV-2-infected individuals [11]. In

90 contrast, we found no evidence for antibodies against ORF3c in SARS-CoV-2 convalescent
91 sera (Fig S1)
92 To characterize the stability and potential activity of cryptic ORF3 peptides, we generated
93 expression vectors for the individual peptides harboring a C-terminal HA-tag (without codon-
94 optimization). Apart from the *ORF3a* construct, *ORF3c* and *ORF3d/ORF3d-2* code for stable
95 proteins that are readily detectable in transfected cells (Fig 1C). The remaining peptides were
96 not (ORF3b-2, ORF3b-3, ORF3b-4) or only poorly (ORF3b, ORF3e) detectable.
97 Since several accessory proteins of SARS-CoV-2 (e.g., ORF3b, ORF6) have been shown to
98 suppress the induction of interferons [1, 12, 13], we hypothesized that some of the cryptic ORF3
99 peptides may exert similar immune-modulatory activities. Indeed, a luciferase reporter assay
100 revealed that ORF3c significantly suppresses the activation of the IFN-β promoter in response
101 to a constitutively active mutant of the pattern recognition receptor RIG-I (Fig 1D). Notably,
102 ORF3c was also more active than the previously described IFN antagonist ORF3b, which
103 suppressed IFN-β promoter activity only at higher concentrations or upon codon-optimization
104 [1]. To test whether ORF3c is able to suppress immune activation upon viral infection, we
105 monitored endogenous *IFNB1* expression upon infection with Sendai virus (SeV), a potent
106 inducer of RIG-I-mediated type I IFN expression [14]. As expected, SeV induced *IFNB1*
107 expression in a dose-dependent manner (Fig 1E). However, *IFNB1* mRNA levels were reduced
108 by about 70% in the presence of SARS-CoV-2 ORF3c.
109 To definitely prove that ORF3c is produced in SARS-CoV-2-infected cells, we monitored its
110 expression at different time points post infection via Western blot. Due to the lack of ORF3c-
111 specific antibodies, we used circular polymerase extension reaction (CPER) [15] to generate a
112 SARS-CoV-2 variant expressing C-terminally HA-tagged ORF3c. Although addition of the HA
113 tag also resulted in the insertion of ten additional amino acids within ORF3a, the rescued virus
114 grew to high titers, similar to the wt virus (not shown). Most importantly, ORF3c-HA was
115 readily detectable in CaCo-2 cells, 24 h and 48 h post infection (Fig 1F). To our knowledge this

116 is the first direct detection of ORF3c in SARS-CoV-2 infected cells. Together, these findings
117 show that SARS-CoV-2 *ORF3c* encodes a stable peptide that suppresses the production of IFN-
118 β upon viral sensing.
119
120 **ORF3c targets MAVS and suppresses both RIG-I- and MDA5-mediated immune**
121 **activation**
122 To elucidate the mechanisms underlying the inhibitory activity of ORF3, we analyzed different
123 steps of the innate RNA sensing cascade culminating in the induction of IFN-β expression (Fig
124 2A). The *IFNB1* promoter harbors binding sites for both IRF3 and NF-κB. As expected,
125 disruption of the NF-κB binding site reduced responsiveness to RIG-I-mediated activation (Fig
126 2B). However, ORF3c still dose-dependently reduced promoter activation (Fig 2B),
127 demonstrating that ORF3c does not selectively target NF-κB activation. Next, we activated the
128 sensing cascade at different steps via over-expressing MDA5, MAVS or a constitutively active
129 mutant of IRF3. While ORF3c suppressed MDA5-mediated immune activation (Fig 2C, left
130 panel), it failed to efficiently suppress *IFNB1* promoter activation in response to MAVS or IRF3
131 over-expression (Fig 2C, middle and right panels). Together, these findings suggest that ORF3c
132 targets immune activation upstream or at the level of the signaling adaptor MAVS. In line with
133 this, SARS-CoV-2 ORF3c weakly co-immunoprecipitated with MAVS, while we found no
134 evidence for an interaction with RIG-I, MDA5 or TBK1 (Fig 2D). The modest co-
135 immunoprecipitation of ORF3c was also observed when a MAVS mutant lacking its CARD
136 domain was used for pull-down (Fig 2E), demonstrating that this domain is dispensable for the
137 interaction. We hypothesized that the interaction of ORF3c with MAVS may also affect the
138 binding of RIG-I to MAVS. Indeed, an established bimolecular fluorophore complementation
139 assay [16] showed evidence for reduced RIG-I:MAVS interaction in the presence of SARS-
140 CoV-2 ORF3c (Fig 1F). Intriguingly, we also noted that increasing amounts of ORF3c resulted
141 in the emergence of a C-terminal MAVS fragment of about 9 kDa (Fig 2G). Together, these

142 findings suggest that ORF3c suppresses IFN-β expression by binding to MAVS, preventing its
143 interaction with RIG-I, and/or inducing its C-terminal cleavage.
144
145 **The immunosuppressive activity of ORF3c is conserved among sarbecoviruses**
146 *In silico* analyses of the ORF3 locus revealed that essentially all sarbecoviruses harbor an
147 *ORF3c* gene encoding a 40- or 41-amino-acid peptide [3]. In contrast, the remaining *ORF3*
148 genes are only poorly conserved or vary substantially in their length (Fig 3A). The absence of
149 *ORF3c* from other subgenera of betacoronaviruses suggests that this open reading frame
150 emerged after the divergence of sarbeco- and hibecoviruses. To test whether the
151 immunosuppressive activity of ORF3c is also conserved, we characterized several orthologs
152 representing human and bat isolates of the SARS-CoV- and SARS-CoV-2-like clusters (Fig
153 3B). Titration experiments revealed that all ORF3c peptides tested significantly suppress IFN-β
154 promoter activation (Fig 3C). However, ORF3c of SARS-CoV-2 Wuhan Hu-1 and a closely
155 related bat coronavirus (ZXC21) suppressed IFN-β promoter activation more efficiently than
156 ORF3c of SARS-CoV Tor2 and SARS-CoV-2 BANAL-20-50.
157 To further map residues in ORF3c involved in its immunosuppressive activity, we performed
158 an alanine scan using the Wuhan Hu-1 orthologue (Fig 3D). While all ORF3c mutants tested
159 still reduced IFN-β promoter activity, the double mutants L2A/L3A and I6A/L7A significantly
160 reduced the immunosuppressive effect of SARS-CoV-2 ORF3c. In summary, these results
161 identify residues in the N-terminus of ORF3c that contribute to its inhibitory activity and
162 demonstrate that ORF3c orthologs from different sarbecoviruses suppress the induction of IFN-
163 β, albeit to different degrees.
164
165 **A natural R36I polymorphism does not affect the immunosuppressive activity of ORF3c**
166 Since the emergence of SARS-CoV-2 in 2019, several mutations have occurred throughout the
167 viral genome. One notable mutation is G25563T (Fig 4A), which is found in the beta, eta, iota

168 and mu variants and has been associated with increased transmission fitness [17]. Although
169 G25563T simultaneously introduces non-synonymous mutations in ORF3a (Q57H), ORF3c
170 (R36I) and ORF3d (E31*) (Fig 4A), previous studies focused only on possible phenotypic
171 consequences of the Q57H change in ORF3a. Notably, however, the R36I mutation in ORF3c
172 is predicted to result in a conformational change (Fig 4B) and a transmembrane domain in the
173 C-terminal half of ORF3c (Fig 4C). We therefore analyzed whether the R36I change may affect
174 the subcellular localization and/or immune-suppressive activity of SARS-CoV-2 ORF3c.
175 Immunofluorescence microscopy revealed that ORF3c of the Wuhan-Hu-1 reference strain and
176 a R36I mutant thereof are similarly distributed throughout the cytoplasm (Fig 4D). Moreover,
177 both ORF3c variants dose-dependently suppressed RIG-I-mediated IFN-β promoter activation
178 to a similar extent (Fig 4E). Thus, the G25563T polymorphism of the SARS-CoV-2 beta, eta,
179 iota and mu variants does not seem to alter the IFN-suppressive activity of ORF3c.
180
181 **Some SARS-CoV-2 variants harbor premature stop codons in *ORF3c***
182 To better understand the relevance of an intact *ORF3c* gene for viral spread, we screened the
183 GISAID SARS-CoV-2 sequence repository for PANGO (sub)lineages harboring a premature
184 ORF3c stop codon in at least 20% of the isolates. We identified two mutations fulfilling these
185 criteria: the first one (C25469T) introduces a premature stop codon (Q5*) in ORF3c and an
186 S26L change in ORF3a (Fig 4F). It is present in about 44% of B.1.617 isolates and in almost
187 all sequences of the B.1.617.1 (delta) and B.1.617.2 (kappa) sublineages (Fig 4G). The second
188 mutation (del25498-25530) represents an in-frame deletion in ORF3a and can be found in about
189 80% of all B.1.630 isolates. This deletion results in the loss of the initiation codon of ORF3d
190 and a premature stop codon (Y14*) in ORF3c. The presence of premature ORF3c stop codons
191 in a substantial fraction of B.1.617 and B.1.630 lineages suggests that ORF3c is dispensable for
192 efficient viral replication *in vivo* and/or may be compensated by changes elsewhere in the
193 genome. Notably, however, the analysis of GISAID SARS-CoV-2 sequences also revealed that

194 a subset (~3%) of B.1.617.2 viruses had acquired an additional point mutation that reverted the
195 stop codon at position 5 to a tyrosine (*5Y), thereby reconstituting ORF3c.
196
197 **ORF3c is dispensable for efficient SARS-CoV-2 replication**
198 To assess the importance of *ORF3c* for efficient viral replication, we generated SARS-CoV-2
199 Wuhan Hu-1 variants harboring inactivating mutations in this gene. Introducing premature stop
200 codons into *ORF3c* is not possible without simultaneously introducing non-synonymous
201 mutations in ORF3a and/or ORF3d. We therefore mutated the start codon of ORF3c to
202 threonine (M1T), which resulted in a silent mutation in the overlapping *ORF3a* gene (D22D)
203 (Fig 5A, left panel). After rescue and validating successful introduction of the mutation, we
204 infected CaCo-2 and CaLu-3 cells with an MOI of 0.1. Quantification of SARS-CoV-2 RNA
205 copies in the culture supernatants over a period of three days revealed that ORF3c M1T
206 replicated as efficiently as wild type SARS-CoV-2 (Fig 5A, right panels). In a parallel
207 experiment, we introduced a premature stop codon (Q5*) in ORF3c, mimicking the mutation
208 that can naturally be found in the SARS-CoV-2 delta and kappa variants (Fig 4F, 5B, left panel).
209 Since the respective nucleotide change introduces a S26L mutation in ORF3a, we
210 simultaneously disrupted *ORF3a* by introducing a premature stop codon (R6*) downstream of
211 a methionine and potential alternative start codon at position 5. While loss of ORF3a markedly
212 reduced replicative fitness in CaCo-2 cells, the virus still replicated efficiently in CaLu-3 cells
213 (Fig 5B, right panels). As observed for the ORF3c M1T mutant, introduction of ORF3c Q5*
214 did not significantly affect the replicative fitness of the virus.
215 Since several (accessory) proteins of SARS-CoV-2 have been shown to suppress the induction
216 of IFN-β and/or IFN-β-mediated immune activation [18, 19], we hypothesized that the
217 immunosuppressive effect of ORF3c may be masked by other viral factors. One potent
218 suppressor of IRF3-mediated IFN-β induction is ORF6 [12, 20]. We therefore generated a BAC
219 clone of SARS-CoV-2, in which *ORF6* was replaced by a *YFP* reporter gene, and introduced

220 the ORF3c M1T mutation described above (Fig 5C, left panel). This clone is based on the B.1
221 variant, and therefore additionally harbors the ORF3c R36I mutation described above. Viral
222 spread was monitored by live-cell imaging and quantification of YFP-expressing (i.e. infected)
223 cells. Again, disruption of *ORF3c* did not result in impaired viral spread, and the ORF3c M1T
224 virus replicated as efficiently as its ORF3c wild type counterpart (Fig 5C, right panels). Thus,
225 while ORF3c and its immunosuppressive activity are conserved among sarbecoviruses, the
226 respective gene is dispensable for viral replication in CaCo-2 and CaLu-3 cells.
227

228 **DISCUSSION**

229 Several lines of evidence suggested that the *ORF3c* gene of SARS-CoV-2 codes for a peptide
230 that plays a role in viral replication: (1) the respective open reading frame is conserved in
231 different sarbecoviruses and shows synonymous site conservation [3, 4, 21] (Fig 3), (2)
232 upstream ATGs do not show a strong initiation context and may allow ORF3c translation via
233 leaky scanning [3] (Fig 1), (3) ribosomal profiling and the HLA-II immunopeptidome suggested
234 that ORF3c is translated in SARS-CoV-2 infected cells [2, 10], (4) ORF3c shows a high density
235 of CD8+ T cell epitopes [21], (5) *in silico* analyses predict a conserved transmembrane domain
236 in ORF3c and a potential role as viroporin [3, 5]. Still, the expression of ORF3c in infected
237 cells, its exact function and its contribution to efficient viral replication have remained unclear.
238 Here, we identify ORF3c as an immune evasion factor of SARS-CoV-2 and other
239 sarbecoviruses that inhibits the induction of IFN-β upon activation of innate sensing cascades.
240 The generation of a replication-competent SARS-CoV-2 variant encoding HA-tagged ORF3c
241 allowed us to demonstrate the presence of a stable ORF3c peptide in virus infected cells. Using
242 luciferase reporter assays, we show that ORF3c suppresses activation of the *IFNB1* promoter
243 by the pattern recognition receptors (PRRs) and RNA sensors RIG-I and MDA5. Importantly,
244 ORF3c also significantly reduced the expression of endogenous IFN-β in response to Sendai
245 virus infection, a known inducer of RIG-I sensing [14]. Since ORF3c exerts its inhibitory effect

246 independently of the receptor, it most likely targets a factor further downstream in the signaling
247 cascade. In line with this, co-immunoprecipitation experiments revealed an interaction of
248 ORF3c with the mitochondrial signaling adaptor MAVS. We found no evidence for an
249 interaction with other components of the sensing cascade (i.e. RIG-I, MDA5, or TBK1).
250 Notably, ORF3c failed to prevent *IFNB1* promoter activation if MAVS itself was used as an
251 activator. This lack of inhibition is not merely the result of a saturation effect since MAVS
252 induced the *IFNB1* promoter less efficiently than RIG-I (Fig 2). MAVS is targeted by proteins
253 from different viruses. For example, Influenza A Virus PB1-F2 inhibits innate sensing by
254 binding to MAVS [22] and decreasing the mitochondrial membrane potential [23]. Another
255 example is the NS3/4A serine protease of Hepatitis C virus (HCV), which cleaves MAVS,
256 thereby inhibiting downstream immune activation [24]. Similarly, SARS-CoV-2 ORF10 was
257 recently shown to induce the degradation of MAVS via mitophagy [25]. Further mechanistic
258 analyses revealed that ORF3c induces the proteolytic processing of MAVS, resulting in a C-
259 terminal 9 kDa fragment of this signaling protein (Fig 2G). Furthermore, ORF3c reduced the
260 interaction of MAVS with RIG-I (Fig 2F). Thus, one possible mode of action is a competitive
261 binding of ORF3c and RIG-I (and possible MDA5) to MAVS. In the presence of ORF3c, the
262 CARD domain of MAVS may not be accessible and thus not be bound and activated by active
263 RIG-I or MDA5. Notably, however, co-immunoprecipitation experiments showed that the
264 CARD domain of MAVS is dispensable for an interaction of ORF3c with MAVS (Fig 2E).
265 In line with a relevant role of ORF3c in viral replication, its immunosuppressive activity is
266 conserved in orthologs of other sarbecovirus species, including the SARS-CoV reference virus
267 Tor2. While all orthologs tested inhibited *IFNB1* promoter activation, those of SARS-CoV Tor2
268 and batCoV BANAL20-52 were less active than their counterparts from SARS-CoV-2 Wuhan-
269 Hu-1 and batCoV ZXC21. The reduced activity of BANAL-20-52 ORF3c can be ascribed to a
270 single amino acid change (L11P) distinguishing it from Wuhan-Hu-1 ORF3c (Fig 3B). While
271 L11 is largely conserved in the SARS-CoV-2 cluster, most of the viruses in the SARS-CoV

272 cluster (including Tor2) harbor a glutamine at this position (Fig 3B) [3, 5]. Thus,
273 polymorphisms at position 11 can affect the inhibitory activity of ORF3c. In addition to this,
274 our alanine scanning approach revealed that Leu2/Leu3 and Ile6/Leu7 are also contributing to
275 the immunosuppressive effect of ORF3c (Fig 3D). Most of these residues are conserved among
276 different sarbecoviruses. One notable exception is Ile6 (Fig 3B). Viruses from the SARS-CoV
277 cluster harbor a Valine at this residue. These include SARS-CoV Tor2 ORF3c, which was less
278 active than its SARS-CoV-2 counterpart.
279 ORF3c is not the only SARS-CoV-2 protein that interferes with RIG-I- and/or MDA-5-
280 mediated immune activation. As already mentioned above, ORF10 suppresses innate sensing
281 by targeting MAVS [25]. Moreover, ORF3b, nucleocapsid, ORF6 and ORF8 have all been
282 shown to suppress IFN-β expression [1, 12, 20, 26, 27], highlighting the selection pressure
283 exerted by this pathway. The convergent evolution of viral proteins exerting overlapping
284 immune evasion activities may represent a backup mechanism that allows viral replication even
285 if one of the IFN-β suppressing proteins is lost. In line with this, SARS-CoV-2 variants
286 expressing a C-terminally truncated, inactive ORF6 protein have emerged several times during
287 the pandemic and spread via human-to-human transmission [12]. Similarly, natural SARS-
288 CoV-2 variants lacking an intact ORF3c gene still efficiently spread in the human population.
289 In fact, more than 80% of the sequenced genomes of B.1.617.1, B.1.617.2 and B.1.630 harbor
290 premature stop codons at positions 5 and 15, respectively (Fig 4). We hypothesized that the loss
291 of ORF3c in these viruses may be compensated by the activity of ORF6. However, replication
292 kinetics in CaCo-2 and CaLu-3 cells revealed that loss of ORF3c does not affect viral
293 replication in the absence of ORF6 either (Fig 5). Intriguingly, IFN-β mRNA levels were not
294 increased upon infection with the SARS-CoV-2 double mutant lacking ORF3c and ORF6 (data
295 not shown). Thus, yet another viral inhibitor of IFN-β expression (e.g. ORF8 or N) may be able
296 to rescue efficient viral replication in this case.

297 Notably, the emergence of premature stop codons in small reading frames such as *ORF3c* may
298 also be tolerated or even be beneficial if they provide a fitness advantage by optimizing
299 overlapping reading frames. For example, the ORF3c Q5* mutation is accompanied by an S26L
300 change in ORF3a. However, experimental disruption of ORF3c without changing the amino
301 acid sequence of ORF3a (Fig 5A) or upon deletion of ORF3a (Fig 5B) did not affect viral
302 replication *in vitro* either.
303 One intriguing observation is the emergence of a nucleotide change in a subfraction (~3%) of
304 B.1.617.2 viruses that reverts the stop codon at position 5 to a tyrosine (*5Y). Thus, it is
305 tempting to speculate that the loss of ORF3c was initially just carried along with mutations
306 elsewhere in the genome (e.g. in Spike) that conferred a major fitness advantage to the virus,
307 before ORF3c expression was reverted by another point mutation.
308 In summary, our study identifies ORF3c as an immune evasion factor of SARS-CoV-2 and
309 other sarbecoviruses. While an intact ORF3c gene is clearly dispensable for viral replication *in*
310 *vitro* and *in vivo*, the conservation of this short open reading frame and the pseudo-reversion of
311 premature stop codons suggests that it may still contribute to efficient viral replication *in vivo*.
312 The emergence of future SARS-CoV-2 variants may help to fully decipher the role of this
313 enigmatic ORF and its co-evolution with other viral genes.
314

315 # MATERIAL & METHODS

316

317 **Generation of expression plasmids**

318 ORF3c genes were PCR-amplified using viral cDNA as a template and subsequently inserted
319 into a pCG expression vector co-expressing GFP via an IRES using unique XbaI and MluI
320 restriction sites. To facilitate protein detection, a C-terminal HA-tag
321 (TACCCATACGATGTTCCAGATTACGCT) was added by extension PCR. To generate

322 ORF3c-HA alanine mutants as well as ORF3c-R36I, -BANAL-20-52, -Tor2 and SL-
323 CoVZXC21, point mutations were introduced by site-directed mutagenesis using the wild type
324 Wuhan-Hu-1 ORF3c-HA expression plasmid as template. pRen2-ORF3c was generated by
325 conventional cloning, using the unique EcoRI and XhoI restriction sites in pRen2. IRF3 5D was
326 PCR-amplified using pCAGGS Flag-IRF3 5D as a template and subsequently inserted into
327 pEGFP-C1 via XhoI and EcoRI. All constructs were sequenced to verify their integrity. PCR
328 primers are listed in EV1.
329
330 **Generation and recovery of a recombinant SARS-CoV-2 ORF3 mutant**
331 Stop mutations within ORF3c were introduced into the bacmid pBSCoV2_d6-YFP harboring
332 the SARS-CoV-2 backbone [28] using 2-step Red Recombination [29]. For this purpose, the
333 KanS cassette was amplified from pEP-KanS with the following oligonucleotides:
334 (1) mut3c-fwd: caattggaactgtaactttgaagcaaggtgaaatcaaggaCgctactccttcagattttgAGGATGACG
335 ACGATAAGTAGGG
336 (2) mut3c-rev: gtatcgttgcagtagcgcgaacaaaatctgaaggagtagcGtccttgatttcaccttgctCAACCAATTA
337 ACCAATTCTGATTAG
338 Integrity of the obtained bacterial artificial chromosomes (BAC) and presence of desired stop
339 mutations were confirmed by restriction digestion and next generation sequencing.
340 Recombinant SARS-CoV-2 viruses expressing EYFP instead of the viral ORF6 protein and
341 containing mutations within ORF3c were recovered by transfection of the BACs into HEK293T
342 cells overexpressing viral N protein, ACE2 receptor, and T7 RNA polymerase as described
343 previously [28]. The obtained reporter viruses were further passaged on CaCo-2 cells and viral
344 titers were determined by endpoint titration (see $TCID_{50}$).
345
346 **Generation of recombinant SARS-CoV-2 mutants by circular polymerase extension**
347 **reaction**

348 To generate recombinant SARS-CoV-2 by circular polymerase extension reaction (CPER) [15]
349 nine DNA fragments comprising parts of SARS-CoV-2 (WK-521, PANGO lineage A; GISAID
350 ID: EPI ISL 408667) [30] were generated by PCR using PrimeSTAR GXL DNA polymerase
351 (TAKARA, Cat# R050A). A linker fragment comprising hepatitis delta virus ribozyme, the
352 bovine growth hormone poly A signal and the cytomegalovirus promoter was also prepared by
353 PCR. The ten obtained DNA fragments were mixed and used for CPER. ORF3c mutations were
354 inserted in fragment 9/10 by site-directed overlap extension PCR with the primers listed in EV1.
355 To produce chimeric recombinant SARS-CoV-2, Tetracycline-inducible ACE2 and TMPRSS-
356 expressing IFNAR1-deficient HEK293 (HEK293-C34) cells were transfected with the CPER
357 products using TransIT-LT1 (MirusBio, Cat#2300) according to the manufacturer's protocol.
358 One day post transfection, the culture medium was replaced with Dulbecco's modified Eagle's
359 medium (high glucose) containing 2% FCS, 1% PS and doxycycline. At 7 d post transfection,
360 the culture medium was harvested and centrifuged, and the supernatants were collected as the
361 seed virus. To remove the CPER products (i.e., any SARS-CoV-2 DNA), 1 ml of the seed virus
362 was treated with 2 µl TURBO DNase (Thermo Fisher Scientific, Cat# AM2238) and incubated
363 at 37°C for 1 h. Complete removal of the CPER products (i.e., SARS-CoV-2-related DNA)
364 from the seed virus was verified by PCR. To prepare virus stocks for
365 infection, VeroE6/TMPRSS2 cells (5,000,000 cells in a T-75 flask) were infected with 20-50
366 µl of the seed virus. One-hour post infection, the culture medium was replaced with DMEM
367 (low glucose) containing 2% FBS and 1% PS. Two to four days post infection, the culture
368 medium was harvested and centrifuged, and the supernatants were collected. Viral titers were
369 determined by $TCID_{50}$. To verify the sequence of chimeric recombinant SARS-CoV-2, viral
370 RNA was extracted from the virus stocks using the QIAamp viral RNA mini kit (Qiagen,
371 Cat#74136) and viral genomes were sequenced as described before [31].
372
373 **Tissue culture infectious dose ($TCID_{50}$)**

374 Viral titers were determined as the 50% tissue culture infectious dose. Briefly, one day before
375 infection, VeroE6/TMPRSS2 cells (10,000 cells) were seeded into 96-well plates. Cells were
376 inoculated with serially diluted virus stocks and incubated at 37°C. Four days later, cells were
377 checked microscopically for cytopathic effects (CPE), and $TCID_{50}$/ml was calculated using the
378 Reed–Muench method.
379
380 **SARS-CoV-2 replication kinetics in Vero E6, Caco-2 and Calu-3 cells**
381 One day before infection with CPER-derived SARS-CoV-2 clones, Caco-2 cells (10,000
382 cells/well) or CaLu-3 cells (20,000 cells/well) were seeded into a 96-well plate. Cells were
383 infected with SARS-CoV-2 at an MOI of 0.1 and incubated at 37°C. One hour later, the infected
384 cells were washed and 180 µl of culture medium was added. The culture supernatants and cells
385 were harvested at the indicated timepoints and used for RT–qPCR to quantify the viral RNA
386 copy number. For replication kinetics of BAC-derived SARS-CoV-2 ΔORF6-YFP and SARS-
387 CoV-2 ΔORF6-YFP ΔORF3c, Caco-2 cells (10,000/well) were seeded into a 96-well plate one
388 day prior to infection. Cells were infected in triplicates at an MOI of 0.1 & 0.01 for 1 hour at
389 37°C. After washing and addition of 100 µl fresh culture medium the plates were placed in an
390 Incucyte plate reader and images were taken at the indicated time points for up to 96 hours.
391 The 'Basic Analysis Mode' was applied to quantify virus growth as green area normalized to
392 phase area. Supernatants and cells were harvested at the indicated time points to determine
393 cytokine levels by Cytokine Array and RT-qPCR respectively.
394
395 **RT–qPCR**
396 5 µl culture supernatant was mixed with 5 µL of 2 x RNA lysis buffer [2% Triton X-100,
397 50 mM KCl, 100 mM Tris-HCl (pH 7.4), 40% glycerol, 0.8 U/µL recombinant RNase inhibitor
398 and incubated at room temperature for 10 minutes. RNase-free water (90 µL) was added, and
399 the diluted sample (2.5 µl) was used as the template for real-time RT-PCR performed according

400 to the manufacturer's protocol using the OneStep TB Green PrimeScript PLUS RT-PCR kit
401 (TAKARA, Cat# RR096A) and the following primers: Forward *N*, 5′-AGC CTC TTC TCG
402 TTC CTC ATC AC-3′; and Reverse *N*, 5′-CCG CCA TTG CCA GCC ATT C-3′. The viral
403 RNA copy number was standardized using a home-made standard.
404 *IFNB1* and *GAPDH* RNA levels were determined in cell lysates collected from (1) SARS-CoV-
405 2 ΔORF6-YFP and SARS-CoV-2 ΔORF6-YFP ΔORF3c infected CaCo-2 wild-type cells and
406 (2) transfected HEK293T cells infected with Sendai virus (Cantell Strain) (Charles River,
407 10100774) for 8 hours. Total RNA was isolated using the Viral RNA Mini Kit (Qiagen,
408 Cat#74136) according to the manufacturer's instructions. Genomic DNA was removed using
409 the DNA-free kit (Thermo Fischer Scientific, Cat# AM1906) and subsequent cDNA synthesis
410 was performed using the PrimeScript RT reagent Kit (TAKARA, Cat# RR037A), both
411 according to the manufacturer's instructions. qPCR was performed using the Luna Universal
412 Probe qPCR Master Mix (NEB) together with primer probes for IFN-β (Thermo Fischer
413 Scientific, Cat# 4331182) and GAPDH (Thermo Fischer Scentific, Cat# 4448489). All
414 reactions were run in duplicates and RNA levels were internally normalized to GAPDH.
415
416 **Transfection of HEK293T cells**
417 For overexpression experiments, HEK293T cells were transfected using standard calcium
418 phosphate transfection protocols. 6x 10^5 cells were seeded in 6-well plates on the day before
419 and medium was changed 6 hours after transfection.
420
421 **Bimolecular fluorescence complementation (BiFC) Assay**
422 The BiFC assay was performed essentially as previously described [16]. In brief, HEK293T
423 cells were transfected with a combination of expression plasmids encoding YFP amino acids 1
424 to 154 (yn) or 155 to the end (yc) conjugated to the N-terminus of RIG-I or MAVS, respectively.
425 Cells were additionally transfected with an expression plasmid encoding different variants of

426 ORF3c-HA or an empty vector control as well as an expression plasmid encoding BFP as
427 transfection control (overall ratio: 2:2:1:0.5). After 24 h, cells were fixed using the Fix & Perm
428 Kit 1000 (Nordic-MUbio) according to the manufacturer's instructions. ORF3c-HA was
429 detected using a primary antibody against the HA-tag (Sigma-Aldrich, Cat# H3663) followed
430 by staining with a secondary AF555 antibody (Invitrogen, Cat# A-21422). Samples were
431 measured on a MACS Quant VYB (Miltenyi Biotec). Analysis was performed using FlowLogic
432 V.8 (Inivai) and protein : protein interaction was determined as the MFI of YFP in BFP positive
433 cells.
434
435 **Antibodies**
436 The following primary antibodies were used, Rabbit polyclonal (IgG) anti-HA (1:1000, Sigma-
437 Aldrich, Cat# SAB4300603), Mouse monoclonal anti-HA (1:1000, Sigma-Aldrich, Cat#
438 H3663), Mouse monoclonal (IgG1) anti-Flag (1:1000, Sigma-Aldrich, Cat# F1804), Rabbit
439 polyclonal (IgG) anti-Flag (1:1000, Sigma-Aldrich, Cat# SAB4301135), Rat polyclonal
440 (IgG2a, κ) anti-human GAPDH (1:1000, BioLegend, Cat# 607902), Rabbit polyclonal anti-
441 Sendai Virus (1:2000, MBL Life sience, Cat# PD029), Rabbit monoclonal (IgG) anti-RIG-I
442 (1:1000, Cell Signaling, Cat# 3743), Rabbit monoclonal (IgG) anti-MDA5 (1:1000, Cell
443 Signaling, Cat# 5321), Rabbit monoclonal (IgG) anti-MAVS (1:1000, Cell Signaling, Cat#
444 3993), Rabbit monoclonal (IgG) anti-TBK1 (1:1000), Cell Signaling, Cat# 3504).
445 The following secondary antibodies were used for immunostaining, IRDye® 680RD Goat anti-
446 Mouse IgG (H + L) (1:20000, LI-COR, Cat# 926-68070), IRDye® 680RD Goat anti-Rabbit
447 IgG (H + L) (1:20000, LI-COR, Cat# 926-68071), IRDye® 800CW Goat anti-Mouse IgG (H +
448 L) (1:20000, LI-COR, Cat# 926-32210), IRDye® 800CW Goat anti-Rabbit IgG (H + L)
449 (1:20000, LI-COR, Cat# 926-32211), IRDye® 800CW Goat anti-Streptavidin IgG (H + L)
450 (1:20000, LI-COR, Cat# 926-32230), Alexa Fluor 488 goat anti rabbit IgG (1:250, Invitrogen,
451 Cat# A-11008), Alexa Fluor 488 goat anti mouse IgG (1:250, Invitrogen, Cat# A-11001), Alexa

452 Fluor 555 goat anti mouse IgG (1:250, Invitrogen, Cat# A-21422), Goat anti-Rabbit IgG (H+L)
453 Cross-Adsorbed Secondary Antibody, Alexa Fluor 555 (1:250, ThermoFisher, Cat# A-21428).
454

455 **Co-immunoprecipitation**

456 To investigate possible interactions between ORF3c and proteins of the Interferon signaling
457 pathway, co-immunoprecipitation with subsequent analysis by Western blotting was
458 performed. Briefly, HEK293T cells were seeded in 6-well plates and co-transfected with
459 expression plasmids for HA-tagged ORF3c and Flag-tagged RIG-I, MDA5, MAVS or TBK1
460 (ratio 4:1; 5µg/well). One day post transfection, cells were lysed in 300 µl Western blot lysis
461 buffer and cleared by centrifugation (see "Western blotting"). 45 µl of the lysate was used for
462 whole-cell lysate analysis and further prepared as described in "Western blotting", while 255
463 µl of the lysate was used for co-immunoprecipitation. A pre-clearing step was performed to
464 remove unspecifically binding compounds from the lysate. Pierce Protein A/G Magnetic beads
465 (Thermo Fisher, Cat# 88802) were washed three times with 1 ml NP40 wash buffer (50 mM
466 HEPES, 300 mM NaCl, 0.5% NP40, pH 7.4) and added to the lysate. After incubation for 1 h
467 at 4°C, beads were removed from the lysate using a magnetic rack. To precipitate protein
468 complexes, the lysate was incubated first with an anti-Flag antibody (1.5 µg/sample) for 1 hour
469 followed by addition of 15 µl washed Protein A/G Magnetic Beads for one additional hour at
470 4°C. After incubation, the beads were washed three times in NP40 wash buffer before
471 incubation with 80 µl 1 x Protein Sample Loading Buffer (LI-COR, Cat# 928-40004) at 95°C
472 for 10 minutes to recover bound proteins. After addition of 1.75 ml β-mercaptoethanol, whole-
473 cell lysates and precipitates were analyzed by western blotting.
474

475 **Western blotting**

476 To determine expression of cellular and viral proteins, cells were washed in PBS, lysed in
477 Western blot lysis buffer (150 mM NaCl, 50 mM HEPES, 5 mM EDTA, 0.1% NP40, 500

478 mM Na3VO4, 500 mM NaF, pH 7.5) and cleared by centrifugation at 20,800 x g for 20 min
479 at 4°C. Lysates were mixed with Protein Sample Loading Buffer (LI-COR, Cat# 928-40004)
480 supplemented with 10% β-mercaptoethanol and heated at 95°C for 5 min. Proteins were
481 separated on NuPAGE 4%–12% Bis-Tris Gels (Thermo Fischer Scientific, Cat#
482 NP0323BOX), blotted onto Immobilon-FL PVDF membranes (Merck Milipore, Cat#
483 IPFL00010) and stained using primary antibodies directed against HA-tag, Flag-tag, GAPDH,
484 RIG-I, MDA5, MAVS, TBK1, IRF3 and Infrared Dye labeled secondary antibodies (LI-COR
485 IRDye). Proteins were detected using a LI-COR Odyssey scanner and band intensities were
486 quantified using LI-COR Image Studio Lite Version 5.2.
487
488 **Immunofluorescence microscopy**
489 Confocal immunofluorescence microscopy was used to determine the subcellular localization
490 of ORF3c and ORF3c R36I. Briefly, 150,000 HEK293T cells were seeded on 13 mm diameter
491 glass coverslips coated with poly-L-lysine (Sigma-Aldrich, Cat# P6282-5mg) in 24-well plates.
492 On the following day, cells were transfected with an expression plasmid for ORF3c, ORF3c
493 R36I or an empty vector control (500 ng) using Lipofectamin2000 (Invitrogen, Cat# 11668019).
494 One day post transfection, cells were fixed in 4% PFA for 20 min at RT, permeabilized in PBS
495 0.5% Triton X-100 for 15 min at RT and blocked in 5% BSA/PBS supplemented with 0,1%
496 Triton X-100 for 15 min at RT. ORF3c was stained using a primary antibody against the HA-
497 tag and secondary goat anti-mouse AF555. Nuclei were stained in parallel using 4′,6-
498 Diamidine-2′-phenylindole (DAPI; Thermo Fischer Scientific, Cat# 62247). Coverslips were
499 mounted on glass slides using Mowiol (CarlRoth, Cat# 0713.1) mounting medium and confocal
500 microscopy was performed using an LSM710 (Carl Zeiss).
501
502 **Firefly luciferase assay**

503 HEK293T cells were seeded in 96 well plates at $3x10^4$ cells /well. After 24 h, cells were
504 transfected with a mix of expression vectors containing firefly luciferase reporter constructs for
505 the IFN-β promoter or a mutant thereof lacking NF-κB biding sites (IFN-β ΔNF-κB) (reporter,
506 10 ng), a *Gaussia* luciferase expression plasmid (normalization control, 5 ng), expression
507 plasmids for RIG-I-CARD, MDA5, MAVS or IRF3 5D (stimulus, 5 ng), different amounts of
508 ORF3 expression constructs (12.5 - 100 ng) and empty vector (pCG_HIV-1 M NL4-3 *nef* stop
509 ΔIRES-eGFP) to adjust total DNA amounts across all conditions to 200 ng/well. After 24 h,
510 supernatants were harvested, and cells were lysed in 100µl 1x Passive Lysis Buffer (Promega,
511 Cat# E194A). *Gaussia* luciferase activity in the supernatants was measured by addition of
512 Coelenterazine (PJK Biotech, Cat# 102174). Firefly luciferase activity was measured in the
513 cells using the Luciferase Assay System (Promega, Cat# E1501) according to the manufacturers
514 instruction.
515
516 **LIPS assay**
517 Luciferase fusion protein (10^6 RLU) in 50 µl Buffer A (50 mM Tris, 150 mM NaCl, 0.1% Triton
518 X-100, pH 7.5) and 1 µl sample serum in 49 µl Buffer A was added to 1.5 ml tubes and
519 incubated with shaking at 300 rpm for 1 h at room temperature. Pierce Protein A/G Magnetic
520 beads were added to each condition as a 30% suspension in PBS for an additional hour and
521 shaking at room temperature. Samples were placed on a magnetic rack, and supernatant was
522 removed after 1-minute incubation. Magnetic beads were washed twice with 150 µl Buffer A
523 followed by 2 washes with 150 µl PBS. Samples were transferred into a 96-well opaque nunc-
524 plate (VWR), and 50 µl Coelenterazine (PJK Biotech, Cat# 102174) was added to each
525 condition. Samples were measured immediately on a TriStar² S LB 942 Multimode Reader
526 (Berthold Technologies) with an integration time of 0.1 seconds and a read height of 1 mm.
527
528 **QUANTIFICATION AND STATISTICAL ANALYSIS**

529 Statistical analyses were performed using GraphPad PRISM 9.4.1. For statistical testing
530 between two means P values were calculated using paired or unpaired Student's t test. For
531 comparison within one group, we used one-way analysis of variation (ANOVA) with Dunnett's
532 multiple comparison test and for comparison between two or more groups we used two-way
533 ANOVA with Sidak's multiple comparison test. Unless otherwise stated, data are shown as the
534 mean of at least three independent experiments ± SD. Significant differences are indicated as:
535 * $p \leq 0.05$; ** $p \leq 0.01$; *** $p \leq$ % 0.001 and **** $p \leq 0.0001$. Statistical parameters are
536 specified in the figure legends.
537

538 **ACKNOWLEDGMENTS**

539 We thank Isabell Haußmann for excellent technical assistance and would like to thank the
540 following persons for providing helpful reagents: Peter D Burbelo (LIPS assay plasmids),
541 Konstantin MJ Sparrer (RIG-I, MDA5 and TBK1 expression plasmids, IRF luciferase reporter
542 plasmid), Harmit Malik (MAVS expression plasmid), Rongtuan Lin (IRF3 expression plasmid),
543 Bernd Baumann (NF-κB luciferase reporter plasmid, *Gaussia* luciferase control vector, IKKβ
544 expression plasmid), Michael Gale Jr (IFN-β promoter reporter plasmid), Prof. Takasuke
545 Fukuhara (CPER plasmids and cell lines) and Prof. Takashi Irie (pCAGGS Flag-IRF3 5d).
546 SARS-CoV-2 mNeon Green was kindly provided by Prof. Michael Schindler. We would also
547 like to thank Prof. Adolfo Garcia-Sastre and the CEIRR program (NIAD Centers of Excellence
548 for Influenza Research and Response) for providing BiFC reporter plasmids. This work was
549 funded by the Federal Ministry of Education and Research Germany (BMBF; grant ID: FKZ
550 01KI20135), the Canon Foundation Europe, the Heisenberg Program of the German Research
551 Foundation (DFG; grant ID: SA 2676/3-1) and grants of the COVID-19 program of the Ministry
552 of Science, Research and the Arts Baden-Württemberg (MWK; grants IDs: MWK K.N.K.C.014
553 (U21) and MWK K.N.K.C.015 (U22)) to D.S. AE and AH were supported by BMBF
554 SenseCoV2 01KI20172A; DFG Fokus COVID-19, EN 423/7-1; and Coronavirus research

grants by the Bavarian State Ministry of Science and the Arts and Bavarian State Ministry of Health, Bay-VOC.

AUTHOR CONTRIBUTIONS

M.M. and D.S. conceptualized the study and designed the experiments. M.M. performed most of the experiments. A.H. and A.E. generated and provided BAC clones for SARS-CoV-2 ΔORF6 YFP (ORF3c wild type and ΔORF3). S.F., M.M. and D.S. generated SARS-CoV-2 mutants via CPER that were characterized by D.S., S.F., M.M. and K.U.. C.K. and J.E.K. performed some of the luciferase reporter assays. M.S. sequenced the YFP reporter viruses. A.S. and J.I. performed *in silico* analyses to identify premature stop codons in ORF3c. M.M. and D.S. prepared the figures, and D.S. wrote the initial draft of the manuscript. All authors reviewed and edited the manuscript. A.E., K.S. and D.S. supervised the experiments, provided resources and acquired funding.

DECLARATION OF INTERESTS

The authors declare no competing interests.

REFERENCES

1. Konno Y, Kimura I, Uriu K, Fukushi M, Irie T, Koyanagi Y, Sauter D, Gifford RJ, Consortium U-C, Nakagawa S, *et al.* (2020) SARS-CoV-2 ORF3b Is a Potent Interferon Antagonist Whose Activity Is Increased by a Naturally Occurring Elongation Variant. *Cell Rep* **32**: 108185
2. Finkel Y, Mizrahi O, Nachshon A, Weingarten-Gabbay S, Morgenstern D, Yahalom-Ronen Y, Tamir H, Achdout H, Stein D, Israeli O, *et al.* (2021) The coding capacity of SARS-CoV-2. *Nature* **589**: 125-130
3. Firth AE (2020) A putative new SARS-CoV protein, 3c, encoded in an ORF overlapping ORF3a. *J Gen Virol* **101**: 1085-1089
4. Jungreis I, Sealfon R, Kellis M (2021) SARS-CoV-2 gene content and COVID-19 mutation impact by comparing 44 Sarbecovirus genomes. *Nat Commun* **12**: 2642

586 5. Cagliani R, Forni D, Clerici M, Sironi M (2020) Coding potential and sequence
587 conservation of SARS-CoV-2 and related animal viruses. *Infect Genet Evol* **83**: 104353
588 6. Pavesi A (2020) New insights into the evolutionary features of viral overlapping genes
589 by discriminant analysis. *Virology* **546**: 51-66
590 7. Jungreis I, Nelson CW, Ardern Z, Finkel Y, Krogan NJ, Sato K, Ziebuhr J, Stern-
591 Ginossar N, Pavesi A, Firth AE*, et al.* (2021) Conflicting and ambiguous names of overlapping
592 ORFs in the SARS-CoV-2 genome: A homology-based resolution. *Virology* **558**: 145-151
593 8. Firth AE, Brierley I (2012) Non-canonical translation in RNA viruses. *J Gen Virol* **93**:
594 1385-1409
595 9. Gleason AC, Ghadge G, Chen J, Sonobe Y, Roos RP (2022) Machine learning predicts
596 translation initiation sites in neurologic diseases with nucleotide repeat expansions. *PLoS One*
597 **17**: e0256411
598 10. Weingarten-Gabbay S, Chen DY, Sarkizova S, Taylor HB, Gentili M, Pearlman LR,
599 Bauer MR, Rice CM, Clauser KR, Hacohen N*, et al.* (2023) The HLA-II immunopeptidome of
600 SARS-CoV-2. *bioRxiv*
601 11. Hachim A, Gu H, Kavian O, Mori M, Kwan MYW, Chan WH, Yau YS, Chiu SS, Tsang
602 OTY, Hui DSC*, et al.* (2022) SARS-CoV-2 accessory proteins reveal distinct serological
603 signatures in children. *Nat Commun* **13**: 2951
604 12. Kimura I, Konno Y, Uriu K, Hopfensperger K, Sauter D, Nakagawa S, Sato K (2021)
605 Sarbecovirus ORF6 proteins hamper induction of interferon signaling. *Cell Rep* **34**: 108916
606 13. Miorin L, Kehrer T, Sanchez-Aparicio MT, Zhang K, Cohen P, Patel RS, Cupic A,
607 Makio T, Mei M, Moreno E*, et al.* (2020) SARS-CoV-2 Orf6 hijacks Nup98 to block STAT
608 nuclear import and antagonize interferon signaling. *Proc Natl Acad Sci U S A* **117**: 28344-28354
609 14. Strahle L, Garcin D, Kolakofsky D (2006) Sendai virus defective-interfering genomes
610 and the activation of interferon-beta. *Virology* **351**: 101-11
611 15. Torii S, Ono C, Suzuki R, Morioka Y, Anzai I, Fauzyah Y, Maeda Y, Kamitani W,
612 Fukuhara T, Matsuura Y (2021) Establishment of a reverse genetics system for SARS-CoV-2
613 using circular polymerase extension reaction. *Cell Rep* **35**: 109014
614 16. Sanchez-Aparicio MT, Ayllon J, Leo-Macias A, Wolff T, Garcia-Sastre A (2017)
615 Subcellular Localizations of RIG-I, TRIM25, and MAVS Complexes. *J Virol* **91**
616 17. Oulas A, Zanti M, Tomazou M, Zachariou M, Minadakis G, Bourdakou MM, Pavlidis
617 P, Spyrou GM (2021) Generalized linear models provide a measure of virulence for specific
618 mutations in SARS-CoV-2 strains. *PLoS One* **16**: e0238665
619 18. Min YQ, Huang M, Sun X, Deng F, Wang H, Ning YJ (2021) Immune evasion of
620 SARS-CoV-2 from interferon antiviral system. *Comput Struct Biotechnol J* **19**: 4217-4225
621 19. Xia H, Cao Z, Xie X, Zhang X, Chen JY, Wang H, Menachery VD, Rajsbaum R, Shi
622 PY (2020) Evasion of Type I Interferon by SARS-CoV-2. *Cell Rep* **33**: 108234
623 20. Li JY, Liao CH, Wang Q, Tan YJ, Luo R, Qiu Y, Ge XY (2020) The ORF6, ORF8 and
624 nucleocapsid proteins of SARS-CoV-2 inhibit type I interferon signaling pathway. *Virus Res*
625 **286**: 198074
626 21. Nelson CW, Ardern Z, Goldberg TL, Meng C, Kuo CH, Ludwig C, Kolokotronis SO,
627 Wei X (2020) Dynamically evolving novel overlapping gene as a factor in the SARS-CoV-2
628 pandemic. *Elife* **9**
629 22. Varga ZT, Ramos I, Hai R, Schmolke M, Garcia-Sastre A, Fernandez-Sesma A, Palese
630 P (2011) The influenza virus protein PB1-F2 inhibits the induction of type I interferon at the
631 level of the MAVS adaptor protein. *PLoS Pathog* **7**: e1002067
632 23. Varga ZT, Grant A, Manicassamy B, Palese P (2012) Influenza virus protein PB1-F2
633 inhibits the induction of type I interferon by binding to MAVS and decreasing mitochondrial
634 membrane potential. *J Virol* **86**: 8359-66

635 24. Anggakusuma, Brown RJP, Banda DH, Todt D, Vieyres G, Steinmann E, Pietschmann
636 T (2016) Hepacivirus NS3/4A Proteases Interfere with MAVS Signaling in both Their Cognate
637 Animal Hosts and Humans: Implications for Zoonotic Transmission. *J Virol* **90**: 10670-10681
638 25. Li X, Hou P, Ma W, Wang X, Wang H, Yu Z, Chang H, Wang T, Jin S, Wang X*, et al.*
639 (2022) SARS-CoV-2 ORF10 suppresses the antiviral innate immune response by degrading
640 MAVS through mitophagy. *Cell Mol Immunol* **19**: 67-78
641 26. Hayn M, Hirschenberger M, Koepke L, Nchioua R, Straub JH, Klute S, Hunszinger V,
642 Zech F, Prelli Bozzo C, Aftab W*, et al.* (2021) Systematic functional analysis of SARS-CoV-2
643 proteins uncovers viral innate immune antagonists and remaining vulnerabilities. *Cell Rep* **35**:
644 109126
645 27. Kopecky-Bromberg SA, Martinez-Sobrido L, Frieman M, Baric RA, Palese P (2007)
646 Severe acute respiratory syndrome coronavirus open reading frame (ORF) 3b, ORF 6, and
647 nucleocapsid proteins function as interferon antagonists. *J Virol* **81**: 548-57
648 28. Herrmann A, Jungnickl D, Cordsmeier A, Peter AS, Uberla K, Ensser A (2021) Cloning
649 of a Passage-Free SARS-CoV-2 Genome and Mutagenesis Using Red Recombination. *Int J*
650 *Mol Sci* **22**
651 29. Tischer BK, von Einem J, Kaufer B, Osterrieder N (2006) Two-step red-mediated
652 recombination for versatile high-efficiency markerless DNA manipulation in Escherichia coli.
653 *Biotechniques* **40**: 191-7
654 30. Matsuyama S, Nao N, Shirato K, Kawase M, Saito S, Takayama I, Nagata N, Sekizuka
655 T, Katoh H, Kato F*, et al.* (2020) Enhanced isolation of SARS-CoV-2 by TMPRSS2-expressing
656 cells. *Proc Natl Acad Sci U S A* **117**: 7001-7003
657 31. Kimura I, Yamasoba D, Nasser H, Zahradnik J, Kosugi Y, Wu J, Nagata K, Uriu K,
658 Tanaka YL, Ito J*, et al.* (2022) The SARS-CoV-2 spike S375F mutation characterizes the
659 Omicron BA.1 variant. *iScience* **25**: 105720
660 32. Camproux AC, Gautier R, Tuffery P (2004) A hidden markov model derived structural
661 alphabet for proteins. *J Mol Biol* **339**: 591-605
662 33. Krogh A, Larsson B, von Heijne G, Sonnhammer EL (2001) Predicting transmembrane
663 protein topology with a hidden Markov model: application to complete genomes. *J Mol Biol*
664 **305**: 567-80

665

666

667 # FIGURE LEGENDS

668 **Figure 1: Open reading frames in the *ORF3* gene locus and inhibition of IFN-β induction**

669 **by SARS-CoV-2 ORF3c.**

670 **A** Genome organization of SARS-CoV-2 is illustrated on top; overlapping ORFs in the

671 ORF3 locus are shown at the bottom. Vertical grey lines indicate internal ATG codons.

672 Experimentally confirmed translation initiation sites [2] are highlighted by grey triangles.

673 **B** Kozak sequences of the *ORF3c* initiation codon and upstream ATG codons in *ORF3a*

674 are shown. ATG context was determined using TIS predictor (https://www.tispredictor.com/)

675 [9].

676 **C** Western blot analysis of HEK293T cells transfected with two different concentrations
677 of expression plasmids for the indicated ORF3 proteins and peptides. After 24h ORF3a to
678 ORF3e were detected via a C-terminal HA tag. GAPDH served as loading control.
679 **D** HEK293T cells were co-transfected with the indicated ORF3 expression plasmids, a
680 reporter plasmid expressing firefly luciferase under the control of the *IFNB1* promoter and a
681 construct expressing *Gaussia* luciferase under the control of a minimal promoter. To induce
682 immune signaling, half of the samples were additionally co-transfected with an expression
683 plasmid for the CARD domain of RIG-I. One day post transfection, firefly luciferase activity
684 was determined and normalized to *Gaussia* luciferase activity.
685 **E** HEK293T cells were transfected with an expression plasmid for SARS-CoV-2 ORF3c
686 or an empty vector control. 24 hours post transfection, cells were infected with increasing
687 amounts of Sendai virus (SeV) for an additional 8 hours. Cells were lysed to perform either
688 RNA extraction and subsequent qPCR for IFN-β (left panel) or Western blot analysis (right
689 panel).
690 **F** CaCo-2 cells were infected with SARS-CoV-2 wt or SARS-CoV-2 encoding HA-tagged
691 ORF3c at an MOI of 2. 24 and 48 hours post infection, cells were harvested for Western blot
692 analysis. ORF3c expression was detected via the HA tag. SARS-CoV-2 Nucleocapsid and
693 GAPDH served as controls.
694 Data information: In (D–E), data are presented as mean (±SD) of three independent
695 experiments. Multiple comparison within individual reporter assays (D) were determined by
696 one-way ANOVA with Dunnett's test * $p \leq 0.05$; ** $p \leq 0.01$; *** $p \leq$ % 0.001 and **** $p \leq$
697 0.0001. Multiple comparison between groups (E) were determined by two-way ANOVA with
698 Sidak's multiple comparison test; * $p \leq 0.05$; ** $p \leq 0.01$; *** $p \leq$ % 0.001 and **** $p \leq 0.0001$.
699
700 **Figure 2. ORF3c interacts with MAVS and inhibits IFN-β induction independently of the**
701 **pattern recognition receptor.**

702 **A** Cartoon illustrating IRF3- and NF-κB-mediated activation of the *IFNB1* promoter upon
703 RIG-I- or MDA5-mediated sensing.
704 **B** HEK293T cells were co-transfected with increasing amounts of an expression plasmid
705 for SARS-CoV-2 ORF3c, a construct expressing *Gaussia* luciferase under the control of a
706 minimal promoter and a reporter plasmid expressing firefly luciferase under the control of the
707 *IFNB1* promoter (left panel) or a mutant thereof lacking the NF-κB binding site (right panel).
708 Immune signaling was induced by co-transfecting an expression plasmid for the CARD domain
709 of RIG-I. One day post transfection, firefly luciferase activity was determined and normalized
710 to *Gaussia* luciferase activity.
711 **C** HEK293T cells were transfected and analyzed essentially as described in (B). Immune
712 signaling was introduced by co-transfecting expression plasmids for MDA5 (left panel), MAVS
713 (central panel) or a constitutively active mutant of IRF3 (right panel).
714 **D, E** HEK293T cells were co-transfected with expression plasmids for (D) Flag-tagged RIG-
715 I, MDA5, MAVS, TBK1, (E) MAVS or a mutant thereof lacking its CARD domain
716 (MAVSΔCARD) and an expression plasmid for HA-tagged SARS-CoV-2 ORF3c. One day
717 post transfection, cells were lysed. Cell lysates were analyzed by Western blotting, either
718 directly ("input") or upon pull-down using a Flag-specific antibody ("IP").
719 **F** HEK293T cells were transfected with plasmids expressing BFP, ORF3c, the C-terminal
720 part of YFP fused to RIG-I and/or the N-terminal part of YFP fused to MAVS. 24 h later, cells
721 were fixed, and YFP fluorescence was detected by flow cytometry as a reporter for MAVS-
722 RIG-I interaction. Exemplary flow cytometry data are shown on the right.
723 **G** HEK293T cells were transfected with increasing amounts of an expression plasmid for
724 SARS-CoV-2 ORF3c. One day post transfection, cells were lysed for Western blotting. ORF3c
725 was detected via an HA tag, and MAVS was detected with antiserum specific for the C-terminal
726 part of MAVS. GAPDH served as loading control. MAVS bands were quantified and the ratio
727 of the 9 kDa fragment to total MAVS was calculated. One exemplary blot is shown on the left.

728 Data information: In (B, C, F), data are presented as mean (±SD) of three independent
729 experiments. In (G), data are presented as mean (±SEM) of three independent experiments.
730 Multiple comparison within individual reporter assays were determined by one-way ANOVA
731 with Dunnett's test * $p \leq 0.05$; ** $p \leq 0.01$; *** $p \leq$ % 0.001 and **** $p \leq 0.0001$.
732
733 **Figure 3. Conservation of ORF3c and its immunosuppressive activity in sarbecoviruses.**
734 **A** Simplified cartoon illustrating the *ORF3* locus of randomly selected members of the
735 *Sarbeco*-, *Hibeco*- and *Nobecovirus* genera. Open reading frames with a length of at least 30
736 nucleotides are indicated as rectangles. ORF3c is highlighted in dark red.
737 **B** Alignment of ORF3c amino acid sequences of the indicated viral isolates. Members of
738 the SARS-CoV-2 cluster are shown on top, members of the SARS-CoV cluster at the bottom.
739 For the underlined ORF3c sequences, expression plasmids were generated and analyzed for
740 their ability to inhibit *IFNB1* promoter activation in
741 **C** HEK293T cells were co-transfected with increasing amounts of the indicated ORF3c
742 expression plasmids, a reporter plasmid expressing firefly luciferase under the control of the
743 *IFNB1* promoter and a construct expressing *Gaussia* luciferase under the control of a minimal
744 promoter. An expression plasmid for Influenza A virus non-structural protein 1 (NS1) served
745 as positive control. Immune signaling was induced by co-transfecting an expression plasmid
746 for the CARD domain of RIG-I. One day post transfection, firefly luciferase activity was
747 determined and normalized to *Gaussia* luciferase activity.
748 **D** HEK293T cells were co-transfected with expression plasmids and analyzed essentially
749 as described in (C). The respective alanine mutations are indicated in the alignment on the left.
750 Data information: In (C, D), data are presented as mean (±SD) of three independent
751 experiments. Multiple comparison between groups were determined by two-way ANOVA with
752 Sidak's multiple comparison test; * $p \leq 0.05$; ** $p \leq 0.01$; *** $p \leq$ % 0.001 and **** $p \leq 0.0001$.
753

754 **Figure 4. Characterization of naturally occurring variants of SARS-CoV-2 ORF3c.**

755 **A** Cartoon illustrating non-synonymous changes in ORF3a, c and d as a result of the
756 naturally occurring polymorphisms G25563T.

757 **B** Secondary structure of Wuhan Hu-1 ORF3c (red) and the respective R36I variant
758 thereof (blue) as predicted using PEP-FOLD 3 [32].

759 **C** The presence of transmembrane domains in Wuhan Hu-1 ORF3c (left panel) and the
760 respective R36I variant thereof (right panel) was predicted using TMHMM - 2.0 [33].

761 **D** HEK293T cells were transfected with expression plasmids for Wuhan Hu-1 ORF3c or
762 ORF3c R36I. One day post transfection, cells were stained for ORF3c (anti-HA, green) and
763 nuclei (DAPI, blue) (scale bar = 20 µm).

764 **E** HEK293T cells were co-transfected with increasing amounts of the indicated ORF3c
765 expression plasmids, a reporter plasmid expressing firefly luciferase under the control of the
766 *IFNB1* promoter and a construct expressing *Gaussia* luciferase under the control of a minimal
767 promoter. Immune signaling was induced by co-transfecting an expression plasmid for the
768 CARD domain of RIG-I. One day post transfection, firefly luciferase activity was determined
769 and normalized to *Gaussia* luciferase activity.

770 **F** Mutations introducing premature stop codons in ORF3c that can be found in at least
771 20% of the samples of at least one PANGO (sub)lineage.

772 **G** Frequency of the mutations shown in (F) in the PANGO (sub)lineages B.1.617.1
773 (delta), B.1.617.2 (kappa), B.1.617 and B.1.630.

774 Data information: In (E), data are presented as mean (±SD) of three independent
775 experiments. Multiple comparison between groups were determined by two-way ANOVA with
776 Sidak's multiple comparison test; * $p \leq 0.05$; ** $p \leq 0.01$; *** $p \leq$ % 0.001 and **** $p \leq 0.0001$.

777

778

779 **Figure 5. Disruption of ORF3c does not affect SARS-CoV-2 replication in CaCo-2 or**
780 **CaLu-3 cells.**

781 **A** CPER was used to disrupt the start codon of ORF3c (M1T) in SARS-CoV-2 without
782 affecting the amino acid sequence of ORF3a (left panel). CaCo-2 and CaLu-3 cells were
783 infected with ORF3c wild type (red) or ORF3c-mutated (blue) SARS-CoV-2 at an MOI of 0.1.
784 Viral replication was monitored over 72 hours by determining viral RNA copies in the culture
785 supernatants (right panels).

786 **B** CPER was used to introduce a premature stop codon in ORF3c (Q5stop). To avoid any
787 bias by simultaneously changing the protein sequence of ORF3a (S26L), a premature stop
788 codon was also inserted in ORF3a (R6*) (left panel). Viral replication (right panels) was
789 monitored in CaCo-2 and CaLu-3 cells as described in (A).

790 **C** A SARS-CoV-2 BAC clone harboring a disrupted ORF3c (M1T) and expressing YFP
791 instead of ORF6 was generated (left panel). CaCo-2 and CaLu-3 cells were infected with
792 SARS-CoV-2 ΔORF6-YFP (red) or SARS-CoV-2 ΔORF6-YFP ΔORF3c (blue) at an MOI of
793 0.1. Cells were placed in a live cell imaging device, and the area of YFP positive cells over the
794 total area of cells was quantified every 4 hours for 96 hours. Images below graphs show
795 continuous virus spread (green) over the indicated time points from one randomly chosen well.

796 Data information: In (A-C, right panel), data are presented as mean (A, B ±SD and C
797 ±SEM) of three independent experiments. Multiple comparison between groups were
798 determined by two-way ANOVA with Sidak's multiple comparison test; * $p \leq 0.05$; ** $p \leq$
799 0.01; *** $p \leq$ % 0.001 and **** $p \leq 0.0001$.

800

801 **Figure S1: Detection of SARS-CoV-2-specific antibodies via Luciferase**
802 **Immunoprecipitation System (LIPS).**

803 **A** Principle of the LIPS assay: HEK293T cells are transfected with expression plasmids
804 for a viral protein of interest fused to Renilla luciferase. Subsequently, transfected cells are

805 lysed and incubated with serum samples and magnetic beads. Antibodies against viral proteins
806 of interest will cross-link the luciferase-containing proteins with beads and allow magnet-
807 assisted pull-down of both beads and luciferase activity.

808 **B** LIPS-mediated quantification of antibodies against SARS-CoV-2 N (left panel) and
809 ORF3c (right panel) in sera from SARS-CoV-2 naïve and convalescent sera (RLU, relative
810 light units). Each dot represents one independent serum sample. Differences in antibody levels
811 between SARS-CoV-2 naïve and convalescent sera was determined by unpaired student's t-test
812 with Welch's correction; * $p \leq 0.05$, ** $p \leq 0.01$, *** $p \leq 0.001$.

Fig 1

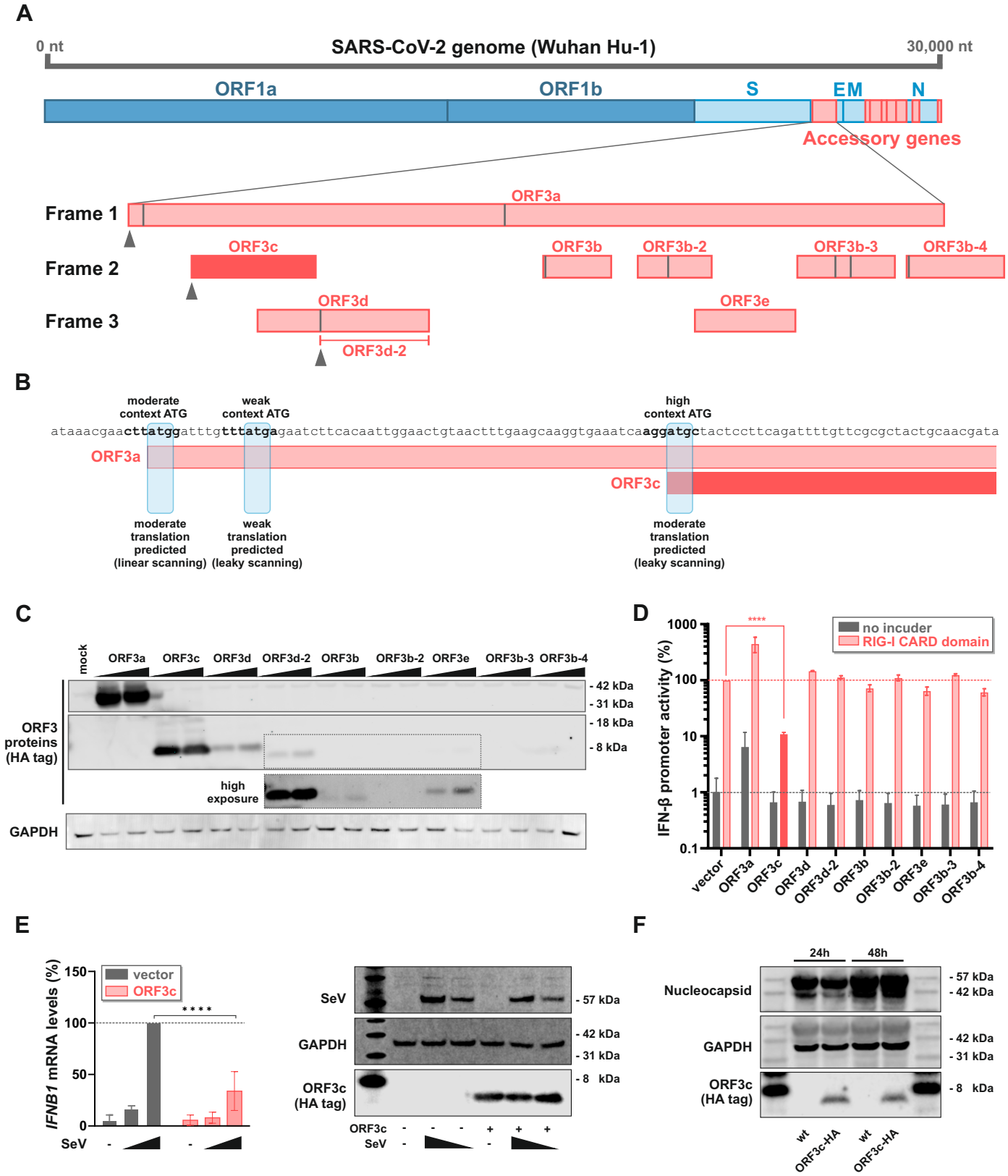
A
0 nt
SARS-CoV-2 genome (Wuhan Hu-1)
30,000 nt
ORF1a
ORF1b
S
EM
N
Accessory genes
Frame 1
ORF3a
Frame 2
ORF3c
ORF3b
ORF3b-2
ORF3b-3
ORF3b-4
Frame 3
ORF3d
ORF3e
ORF3d-2
B
moderate context ATG
weak context ATG
high context ATG
ataaacgaacttatggatttgtttatgagaatcttcacaattggaactgtaactttgaagcaaggtgaaatcaaggatgctactccttcagattttgttcgcgctactgcaacgata
ORF3a
ORF3c
moderate translation predicted (linear scanning)
weak translation predicted (leaky scanning)
moderate translation predicted (leaky scanning)
C
mock
ORF3a
ORF3c
ORF3d
ORF3d-2
ORF3b
ORF3b-2
ORF3e
ORF3b-3
ORF3b-4
ORF3 proteins (HA tag)
high exposure
GAPDH
- 42 kDa
- 31 kDa
- 18 kDa
- 8 kDa
D
no incuder
RIG-I CARD domain
IFN-β promoter activity (%)
1000
100
10
1
0.1
****
vector
ORF3a
ORF3c
ORF3d
ORF3d-2
ORF3b
ORF3b-2
ORF3e
ORF3b-3
ORF3b-4
E
vector
ORF3c
IFNB1 mRNA levels (%)
150
100
50
0
****
SeV
SeV
GAPDH
ORF3c (HA tag)
- 57 kDa
- 42 kDa
- 31 kDa
- 8 kDa
ORF3c
SeV
F
24h
48h
Nucleocapsid
GAPDH
ORF3c (HA tag)
- 57 kDa
- 42 kDa
- 31 kDa
- 8 kDa
wt
ORF3c-HA
wt
ORF3c-HA

Fig 2

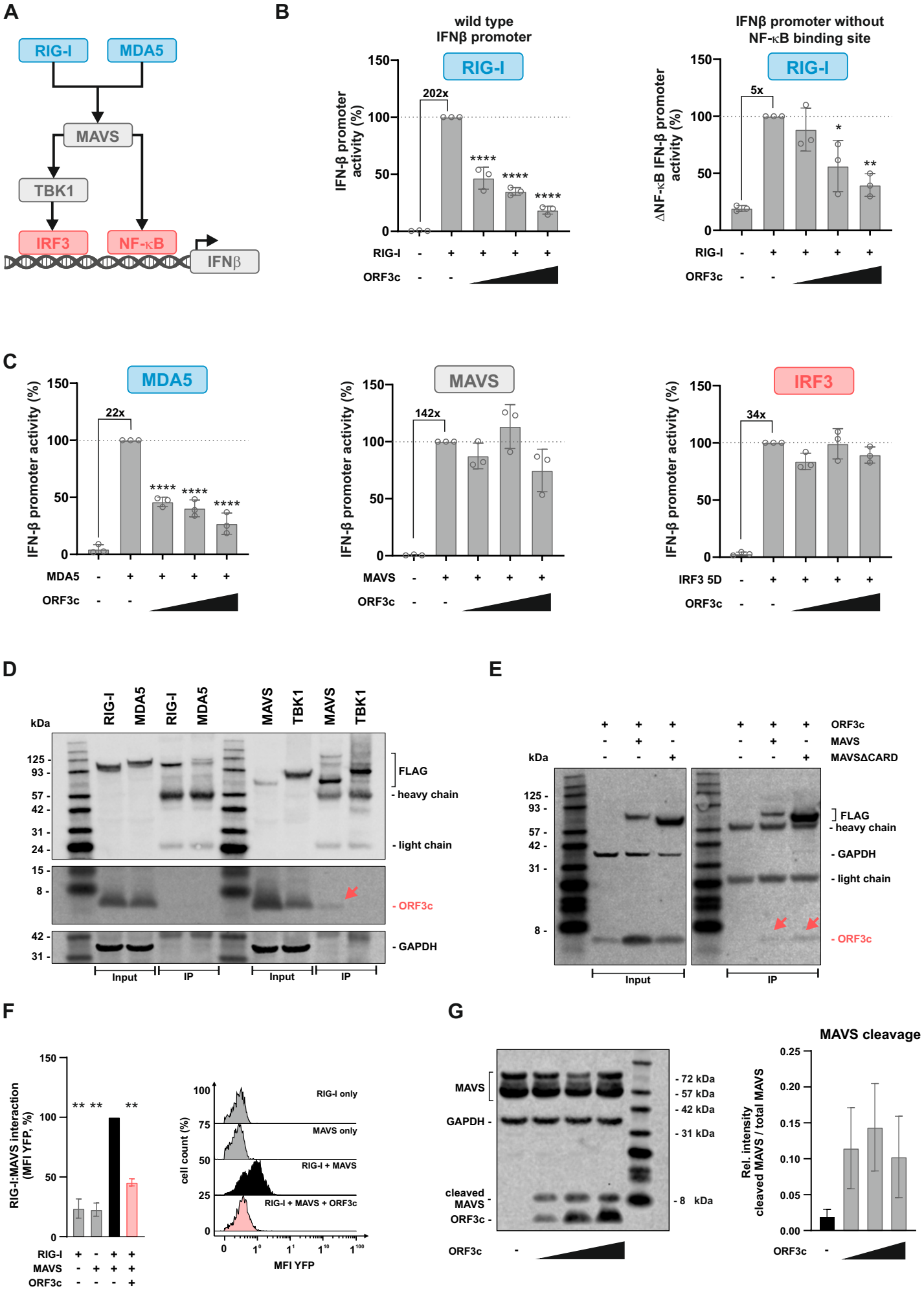
A
RIG-I
MDA5
MAVS
TBK1
IRF3
NF-κB
IFNβ
B
wild type IFNβ promoter
RIG-I
IFN-β promoter activity (%)
202x
RIG-I
ORF3c
IFNβ promoter without NF-κB binding site
RIG-I
ΔNF-κB IFN-β promoter activity (%)
5x
C
MDA5
22x
MAVS
142x
IRF3
34x
IFN-β promoter activity (%)
MDA5
MAVS
IRF3 5D
ORF3c
D
kDa
RIG-I
MDA5
MAVS
TBK1
FLAG
- heavy chain
- light chain
- ORF3c
- GAPDH
Input
IP
E
ORF3c
MAVS
MAVSΔCARD
- GAPDH
F
RIG-I:MAVS interaction (MFI YFP, %)
RIG-I
MAVS
ORF3c
RIG-I only
MAVS only
RIG-I + MAVS
RIG-I + MAVS + ORF3c
cell count (%)
MFI YFP
G
MAVS
GAPDH
cleaved MAVS
ORF3c
- 72 kDa
- 57 kDa
- 42 kDa
- 31 kDa
- 8 kDa
MAVS cleavage
Rel. intensity cleaved MAVS / total MAVS

Fig 3

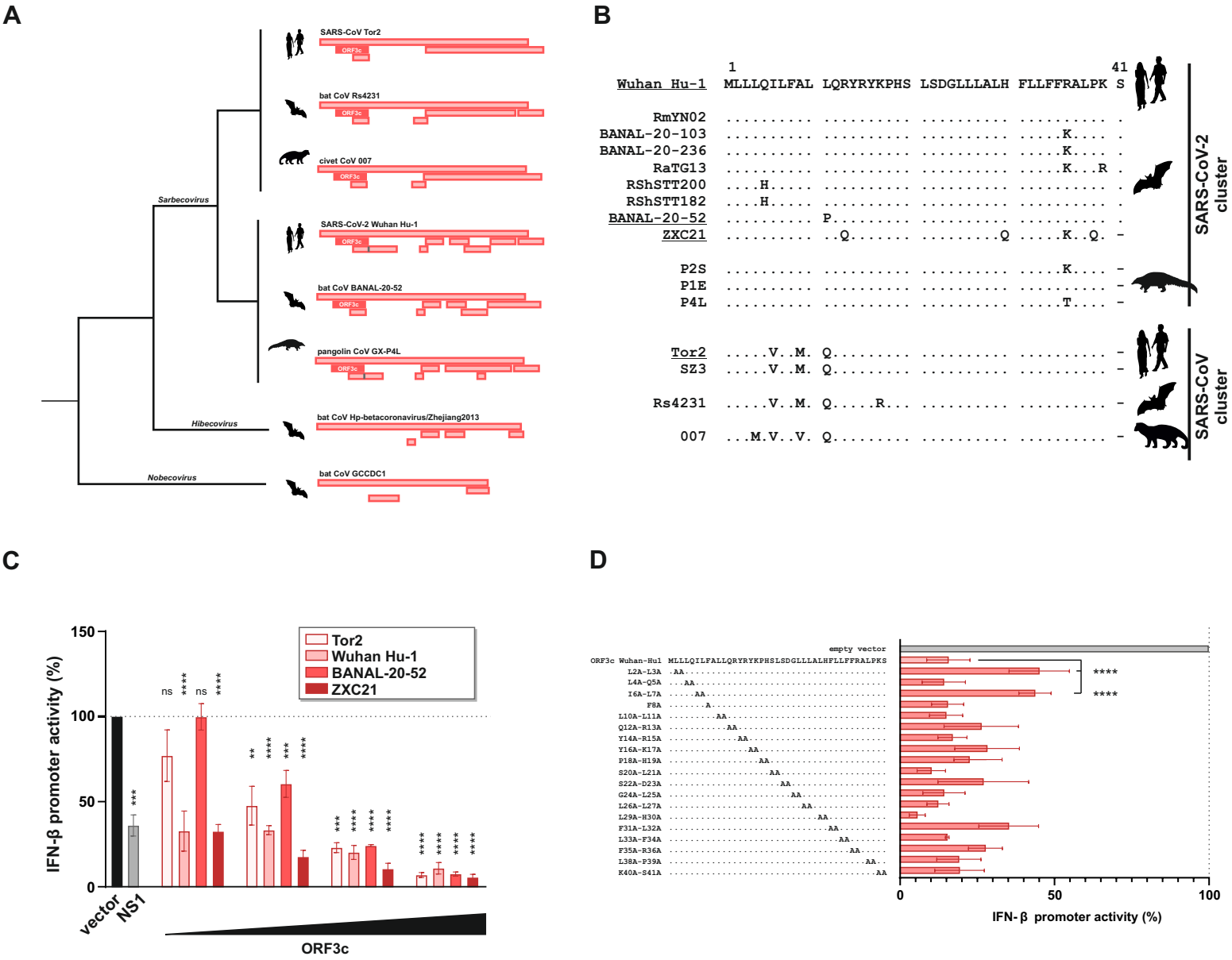
A
SARS-CoV Tor2
bat CoV Rs4231
civet CoV 007
SARS-CoV-2 Wuhan Hu-1
bat CoV BANAL-20-52
pangolin CoV GX-P4L
bat CoV Hp-betacoronavirus/Zhejiang2013
bat CoV GCCDC1
ORF3c
Sarbecovirus
Hibecovirus
Nobecovirus
B
Wuhan Hu-1 MLLLQILFAL LQRYRYKPHS LSDGLLLALH FLLFFRALPK S
RmYN02
BANAL-20-103
BANAL-20-236
RaTG13
RShSTT200
RShSTT182
BANAL-20-52
ZXC21
P2S
P1E
P4L
Tor2
SZ3
Rs4231
007
SARS-CoV-2 cluster
SARS-CoV cluster
C
IFN-β promoter activity (%)
Tor2
Wuhan Hu-1
BANAL-20-52
ZXC21
vector
NS1
ORF3c
D
empty vector
ORF3c Wuhan-Hu1 MLLLQILFALLQRYRYKPHSLSDGLLLALHFLLFFRALPKS
L2A-L3A
L4A-Q5A
I6A-L7A
F8A
L10A-L11A
Q12A-R13A
Y14A-R15A
Y16A-K17A
P18A-H19A
S20A-L21A
S22A-D23A
G24A-L25A
L26A-L27A
L29A-H30A
F31A-L32A
L33A-F34A
F35A-R36A
L38A-P39A
K40A-S41A
IFN-β promoter activity (%)

Fig 4

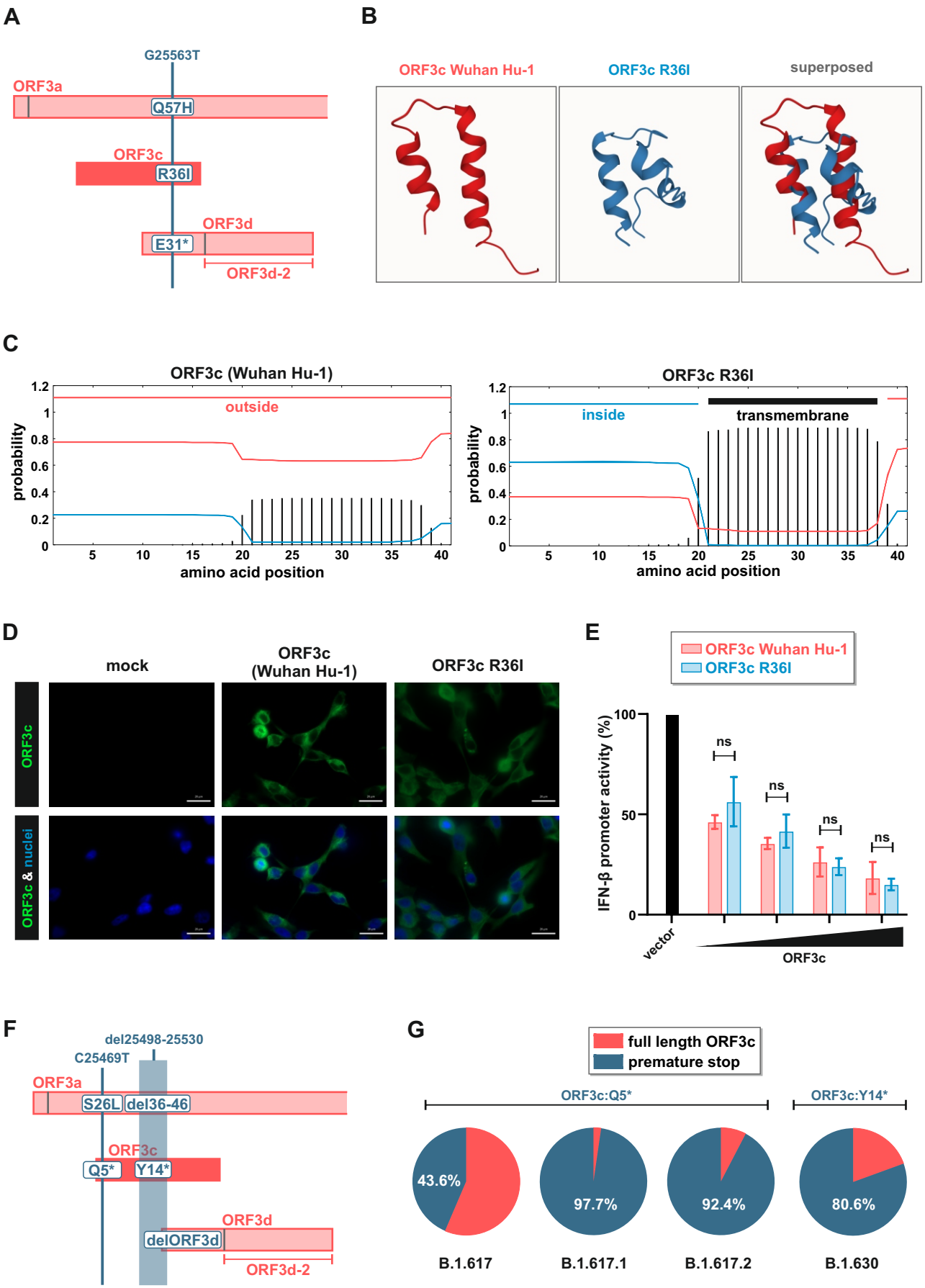
A
G25563T
ORF3a
Q57H
ORF3c
R36I
ORF3d
E31*
ORF3d-2
B
ORF3c Wuhan Hu-1
ORF3c R36I
superposed
C
ORF3c (Wuhan Hu-1)
outside
probability
amino acid position
ORF3c R36I
inside
transmembrane
probability
amino acid position
D
mock
ORF3c (Wuhan Hu-1)
ORF3c R36I
ORF3c
ORF3c & nuclei
E
ORF3c Wuhan Hu-1
ORF3c R36I
IFN-β promoter activity (%)
ns
vector
ORF3c
F
del25498-25530
C25469T
ORF3a
S26L
del36-46
ORF3c
Q5*
Y14*
ORF3d
delORF3d
ORF3d-2
G
full length ORF3c
premature stop
ORF3c:Q5*
ORF3c:Y14*
43.6%
97.7%
92.4%
80.6%
B.1.617
B.1.617.1
B.1.617.2
B.1.630

Fig 5

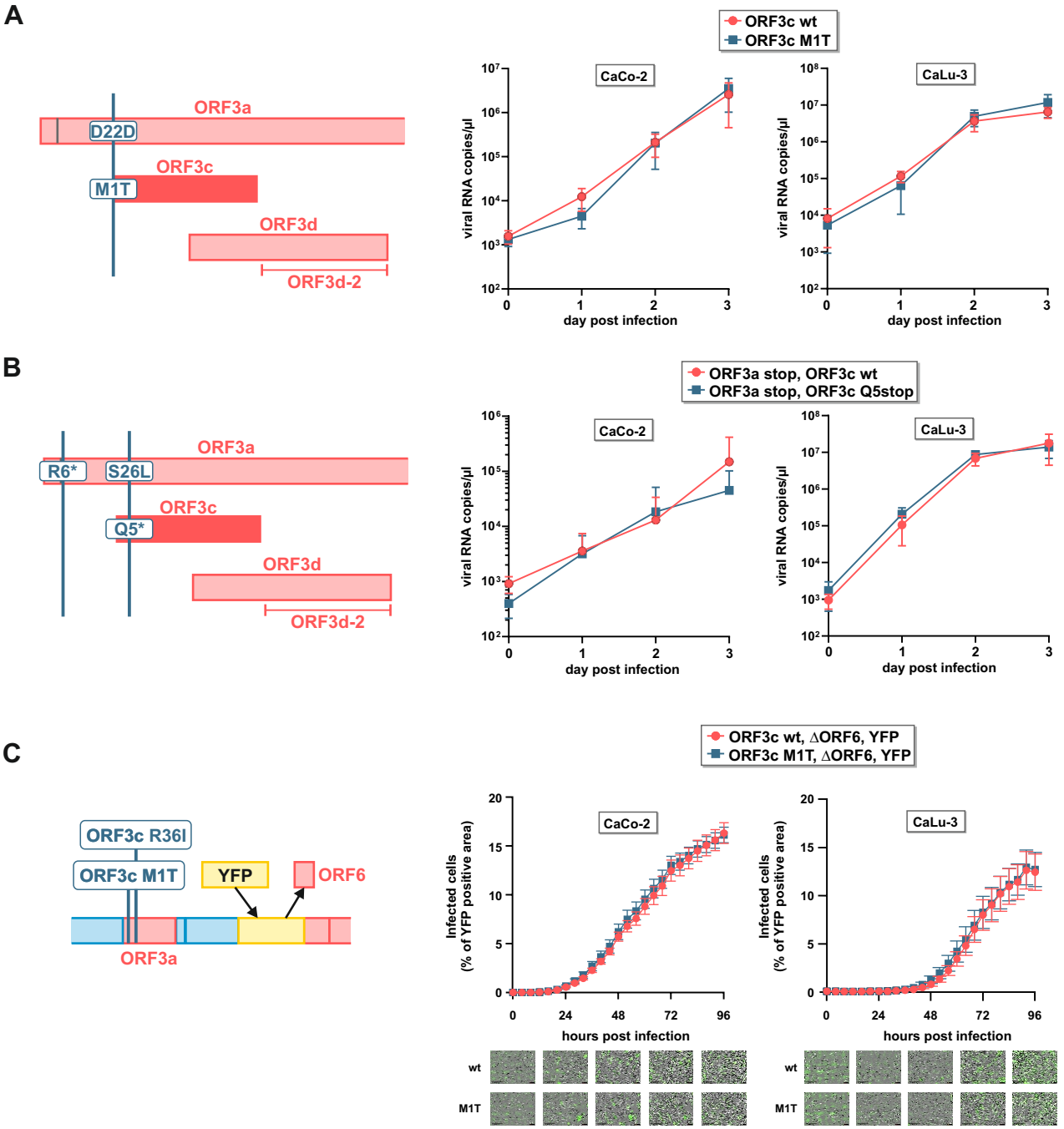
A
ORF3a
D22D
ORF3c
M1T
ORF3d
ORF3d-2
ORF3c wt
ORF3c M1T
CaCo-2
CaLu-3
viral RNA copies/µl
day post infection
B
R6*
S26L
Q5*
ORF3a stop, ORF3c wt
ORF3a stop, ORF3c Q5stop
C
ORF3c R36I
ORF3c M1T
YFP
ORF6
ORF3c wt, ΔORF6, YFP
ORF3c M1T, ΔORF6, YFP
Infected cells
(% of YFP positive area)
hours post infection
wt
M1T